Software-defined radio-based HF doppler receiving system

Hiroyuki Nakata[1*] , Kenro Nozaki[2], Yuhei Oki[1], Keisuke Hosokawa[2], Kumiko K. Hashimoto[3], Takashi Kikuchi[4], Jun Sakai[2], Ichiro Tomizawa[5] and Satoko Saita[6]

Abstract

High-frequency Doppler (HFD) sounding is one of the major remote sensing techniques used for monitoring the ionosphere. Conventional systems for HFDs mainly utilize analog circuits. However, existing analog systems have become difficult to maintain as the number of people capable of working with analog circuits has declined. To solve this problem, we developed an alternate HFD receiver system based on digital signal processing. The software-defined radio (SDR) technique enables the receiver to be set up without the knowledge of analog circuit devices. This approach also downsizes the system and reduces costs. A highly stabilized radio system for both the transmitter and receiver is necessary for stable long-term observations of various phenomena in the ionosphere. The global positioning system disciplined oscillator with an accuracy of 10^{-11} compensates for the frequency stability required by the new receiving system. In the new system, four frequencies are received and signal-processed simultaneously. The dynamic range of the new system is wider (>130 dB) than that of the conventional system used in HFD observations conducted by the University of Electro-Communications in Japan. The signal-to-noise ratio significantly improved by 20 dB. The new digital system enables radio waves to be received with much smaller amplitudes at four different frequencies. The new digital receivers have been installed at some of the stations in the HFD observation network in Japan and have already captured various ionospheric phenomena, including medium-scale traveling ionospheric disturbances and sudden commencement induced electric field fluctuations, which indicates the feasibility of SDR for actual ionospheric observations. The new digital receiver is simple, inexpensive, and small in size, which makes it easy to deploy new receiving stations in Japan and elsewhere. These advantages of the new system will help drive the construction of a wide HFD observation network.

Keywords: Ionosphere, Radio propagation, Software-defined radio, Signal processing

*Correspondence: nakata@faculty.chiba-u.jp
[1] Graduate School of Engineering, Chiba University, Chiba, Japan
Full list of author information is available at the end of the article

Nakata *et al. Earth, Planets and Space*   (2021) 73:209

Page 2 of 16

Graphical Abstract
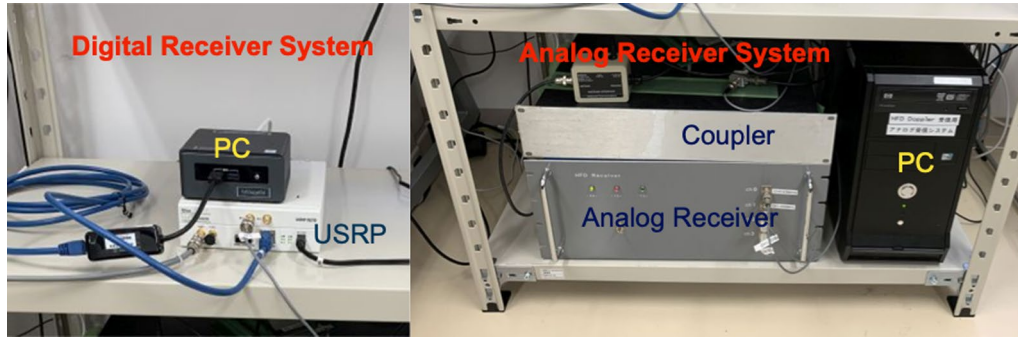
Introduction

To examine the dynamics of the ionosphere, observations of both the steady and disturbed states of the ionosphere are important. Various observation systems have been utilized to observe the structure of the ionosphere and many types of disturbances occurring in the ionosphere. One useful ground-based observation system is high-frequency Doppler (HFD) sounding (e.g., Ogawa 1958; Davies et al. 1962; Jacobs and Watanabe 1966). Utilizing the recent progress in software-define radio, we have developed new digital receivers for the HFD sounding system. The purpose of this paper is to describe the new receiver system, report the results of pilot observations, and discuss its potential use. In the introduction, the principles of the HFD sounding and the history/activities of Doppler observations in various countries are summarized. The motivation for the development of a new digital receiver is also described.

HF band radio waves transmitted from the ground are reflected by ionized plasmas at ionospheric altitudes. When the length of the phase path of the radio wave varies, the frequency of the radio wave shifts owing to the Doppler effect. The frequency variation of the radio wave at the receiving point, Δf, is given by

$$\Delta f = -\frac{f}{c}\frac{d}{dt}\int_0^l ndl, \tag{1}$$

where f is the frequency of the transmitted radio wave, c is the speed of light, n is the refractive index, and l is the distance between the transmitting and receiving points along the ray path (Davies et al. 1962; Jacobs and Watanabe 1966). From this equation, it is recognized that two factors cause the frequency variation of the radio wave. One is the vertical motion of the refection point (the temporal variation of l) and the other is the temporal variation of the refractive index in the propagation path of the radio wave. Here, it is assumed that the radio wave is

reflected at an altitude of h at the midpoint between the transmitter and receiver. When the altitude of the reflection point moves upward by $\Delta h(\ll h)$, and the refractive index does not vary along the propagation path, the variation of the phase path of the radio wave (the integral of the refractive index) corresponds to the variation of the propagation path. Therefore, the variation of the phase path, Δn, is expressed as (Davies et al. 1962):

$$\Delta n = 2\Delta h\cos\theta. \tag{2}$$

Here, θ is the incident angle of the radio wave to the ionosphere. Using Eqs. (1) and (2), the relationship between the frequency variation (Doppler frequency) and the vertical speed of the reflection point, v_h, is given by

$$\Delta f = -2\frac{f\cos\theta}{c}\frac{dh}{dt} = -2\frac{f\cos\theta}{c}v_h. \tag{3}$$

Using this equation, we can estimate the vertical motion of ionospheric plasma from the Doppler frequency. The Doppler frequency is also affected by the temporal variation of the refractive index on the propagation path. If the earth's magnetic field and the collision of the particles are neglected for simplicity, the refractive index is given by

$$n = \sqrt{1 - \frac{f_p^2}{f^2}} = \sqrt{1 - \frac{e^2}{4\pi^2\varepsilon_0 m}\frac{N}{f^2}}, \tag{4}$$

where f_p is the plasma frequency, e is the elementary charge, ε_0 is the permittivity of the vacuum, m is the mass of an electron, and N is the electron density. As a result, the temporal variation of the electron density distribution introduces the frequency variation of the radio waves through the variation of the refractive index. In this case, the variation of the phase path is given by

Nakata *et al. Earth, Planets and Space* (2021) 73:209

Page 3 of 16

$$\frac{d}{dt}\int_0^l n\,dl = 2\int_0^h \frac{\partial n}{\partial t}\,dh = -\frac{e^2}{4\pi^2\varepsilon_0 m}\frac{1}{f^2}\int_0^h \frac{1}{n}\frac{\partial N}{\partial t}\,dh. \tag{5}$$

Using Eqs. (1) and (5), the frequency variation of the radio wave is expressed as (Davies et al., 1962; Jacobs and Watanabe, 1966; Chum et al., 2012, 2016):

$$\Delta f = \frac{e^2}{4\pi^2\varepsilon_0 mcf}\int_0^h \frac{1}{n}\frac{\partial N}{\partial t}\,dh. \tag{6}$$

There are many possible causes for the temporal variation in the electron density distribution. Compressional waves, such as sound waves, are one of the major factors. Assuming that the ionospheric plasmas are dragged by the neutral atmospheric particles due to collisions, we can estimate the amplitude of the atmospheric wave using HFD observations. For the derivation of the amplitude of the acoustic wave in detail, see Chum et al. (2012, 2016).

Since the basics of HFD sounding were invented by Ogawa (1958), the initial HFD observation in Japan was carried out by researchers at Doshisha University. Ichinose and Ogawa (1974) examined the vertical motion of the ionosphere using HFD observations and showed that the derivative of the horizontal component of the geomagnetic field varied in phase with the Doppler frequency during a sudden commencement (SC). Concerning the internal gravity waves caused by a solar eclipse, Ichinose and Ogawa (1976) showed that fluctuations with a period of 22 min appeared on the day of a solar eclipse. The University of Electro-Communications (UEC) and the Radio Research Laboratory (RRL, now the National Institute of Information and Communications Technology) have also promoted HFD sounding in Japan. At UEC, the ionospheric disturbances in the lower atmospheres have been extensively examined, such as acoustic gravity waves (AGWs) (Shibata and Okuzawa 1983; Shibata 1986), earthquakes (Okuzawa et al. 1983), and typhoons (Okuzawa 1986). At RRL, Kikuchi et al. (1985) and Kikuchi (1986) focused on the storm-time variations in the electric field in the ionosphere.

In these earlier observations, Japan standard time and frequency signal emission (call sign: JJY) at frequencies of 5000 and 8000 kHz were used. However, the transmission of JJY shifted from the HF band to the LF band at the end of March 2001, and the transmission of JJY at 5000 and 8000 kHz was terminated. To maintain the HFD observations in Japan, since 2001, UEC has started transmitting alternative HF radio waves at two frequencies (5006 kHz and 8006 kHz) (Tomizawa et al. 2003) and installed receivers in several places in Japan. Later, the HFD receiving systems at several observation points were upgraded to receive two additional

radio waves from the commercial broadcasting of Radio NIKKEI (6055 kHz and 9595 kHz) transmitted from the Nagara transmitter. By receiving radio waves at four different frequencies, we were able to observe ionospheric fluctuations at four different altitudes (the transmission of radio waves at 9595 kHz stopped on 01 October 2018).

Even in recent years, HFD data provided by this network have been used in many studies. Kikuchi et al. (2016, 2021) examined the response of the ionosphere to SC and showed that the vertical motion of the ionosphere is well explained by the potential electric field transmitted from the high-latitude ionosphere. Hashimoto et al. (2020) also examined the prompt penetration of electric fields during an intense geomagnetic storm on 22 June 2015. In combination with the HFD data obtained by the Institute of Atmospheric Physics (IAP) in the Czech Republic, Hashimoto et al. (2020) showed the penetration of an eastward electric field in the evening and a westward electric field at night during the main phase of the storm. Taking advantage of the ability to receive radio waves at four different frequencies, Nakata et al. (2021) examined coseismic ionospheric disturbances observed at different altitudes in association with the foreshock of the Tohoku Earthquake and demonstrated that coseismic disturbance was caused by the vertical propagation of the acoustic mode wave.

HFD sounding systems have been developed worldwide. A group at the IAP has constructed a network of HFD sounding systems globally (Laštovička and Chum, 2017). Over hundreds of square kilometers, transmitter/receiver networks have been constructed in the Czech Republic, South Africa, Taiwan, and France. The details and outcomes of this system were reviewed by Laštovička and Chum (2017). In the case of this HFD system, because the transmitters and the receiver are closely located, the vertical speed of the motion of the reflection point can be determined accurately. Farges et al. (2003) installed an HFD sounding system in the north of France and carried out continuous observations using three receivers at a distance of 50 to 80 km. The generation of atmospheric waves in association with a solar eclipse was examined using this system. This system has also been used to study the ionospheric signatures of Rayleigh waves in association with over-the-horizon radar (Occhipinti et al. 2010). Mainly to observe the ionospheric disturbances associated with earthquakes, Doppler observations have been conducted by several universities in Taiwan, covering the entire island of Taiwan (Liu et al. 2016). In India, a single frequency HFD radar was installed in 1982, and a multi-frequency Doppler radar (2.5 MHz, 3.5 MHz, and 4.5 MHz) was developed in 2003 (Simi et al. 2020). The data obtained by this system have proven useful for

Nakata *et al. Earth, Planets and Space* (2021) 73:209

Page 4 of 16

many types of research, including studies of plasma drift in low-latitude regions.

Several other radio instruments can observe frequency variations as well as HFD sounding. Reinish et al. (2009) improved the hardware and software of the digisonde to observe the angles of arrival (AoA), time of flight, and Doppler frequency of reflected radio signals. Reinish et al. (2018) constructed an oblique ionosonde network and specified the wave parameters of traveling ionospheric disturbances (TIDs) using the AoA and Doppler frequency obtained by the ionosonde observation of the bistatic digisonde network. The Super Dual Auroral Radar Network (SuperDARN) radars (Greenwald et al. 1995) are capable of obtaining many types of ionospheric data, including Doppler frequency (Chisham et al. 2007; Nishitani et al. 2019). Basically, the SuperDARN radar observes coherent scatter from field-aligned irregularities (FAI) in the ionosphere. The Doppler velocity of such ionospheric echoes corresponds to the line-of-sight component of plasma drift perpendicular to the electric and magnetic fields. The ground scatter echoes reflect the vertical motion and incident angle variation of the bottom side of the ionosphere. In the case of sea scatter, an additional surface wave spectrum may be supplied by the Doppler shift (Anderson 2019; Skolnik 1990).

As long as stable and accurate transmitters are prepared, the HFD sounders have the advantage of observing the motion of the ionosphere with high temporal resolution (e.g., 10 s) at a fixed point. The frequency variation of the HF band radio wave is very small (usually less than several Hz) in actual observations (e.g., Davies and Baker 1966; Laštovička and Chum 2017). To detect such small frequency variations in HFD soundings, it is necessary to transmit continuous high-frequency waves accurately and stably.

Recently, software-defined radio (SDR) has become widely used for radio observations in the ionosphere. Bostan et al. (2019) developed an inexpensive SDR-based ionospheric sounding system. The system, which was mostly constructed with commercial off-the-shelf products and open-source software, performed satisfactorily. Ivanov et al. (2015) demonstrated that the SDR HF band frequency modulated continuous wave (FMCW) oblique ionosonde receiver based on SDR has higher noise immunity and reliability than the analog receiver over a propagation distance of 3000 km. SDR-based receivers, such as universal software radio peripheral (USRP), have become more reliable. They are now being deployed as synthesizers and receiver systems in SuperDARN radars, as reported by Bristow (2019).

Our current HFD observation system has been operating since 2001, without any significant hardware changes. Recently, however, continuous operation and maintenance of the system have become difficult owing to the aging of transmission and reception systems. Because of the progress of SDR, a new receiving system for HFD soundings can be developed as a digital receiver. As will be detailed later, the advantages of the use of SDR are: (1) flexible selection of observation frequency and/or filter bandwidth; (2) commercial-off-the-shelf components and relatively lower cost of equipment development using open-source software; (3) much smaller equipment size; and (4) development of a new system without sufficient knowledge of analog circuits. While the conventional analog receiver is controlled by the performance of the analog devices, the performance of the digital receiver depends on the data processing capability of the personal computer (PC) incorporated in the SDR. The decreasing cost and size of the processing PC are also the advantages of SDR, which enable the new receiving system to be transported as hand luggage.

Based on the foregoing, we developed a new digital receiving system for HFD observations. As will be described later, we succeeded in developing a new receiving system with a higher performance than conventional analog receivers. Guo et al. (2019) developed a similar observation system using USRP, in which dedicated software was installed to receive radio waves at multiple frequencies simultaneously. Unfortunately, the detailed characteristics of the receiver using USRP have not yet been clarified. Therefore, we will examine the characteristics of the new digital receiver in detail.

In this paper, we describe the details of the newly developed digital receiving system in comparison with a conventional analog system. We also introduce simultaneous observations made using both analog and digital systems in Awaji, Japan, to evaluate the performance of the new system. The results of this simultaneous observation confirm that the new digital system has sufficient performance for HFD observations of ionospheric phenomena and is quite useful for actual observations.

Observation systems

In this section, we introduce both a conventional receiving system using analog circuits and the newly developed digital system. As described above, both systems receive four different radio waves with carrier frequencies of 5006, 6055, 8006, and 9595 kHz. Table 1 shows a list of transmitters used in the HFD sounding in Japan. The monochromatic signals at frequencies of 5006 kHz and 8006 kHz (call sign: JG2XA) with a power of 200 W are regulated at the transmitter side by a Rubidium (Rb) oscillator and transmitted from the Chofu campus of UEC (35.657 N, 139.543E) (Tomizawa et al. 2003). The radio waves at frequencies of 6055 kHz and 9595 kHz are transmitted from the Nagara transmitter of commercial
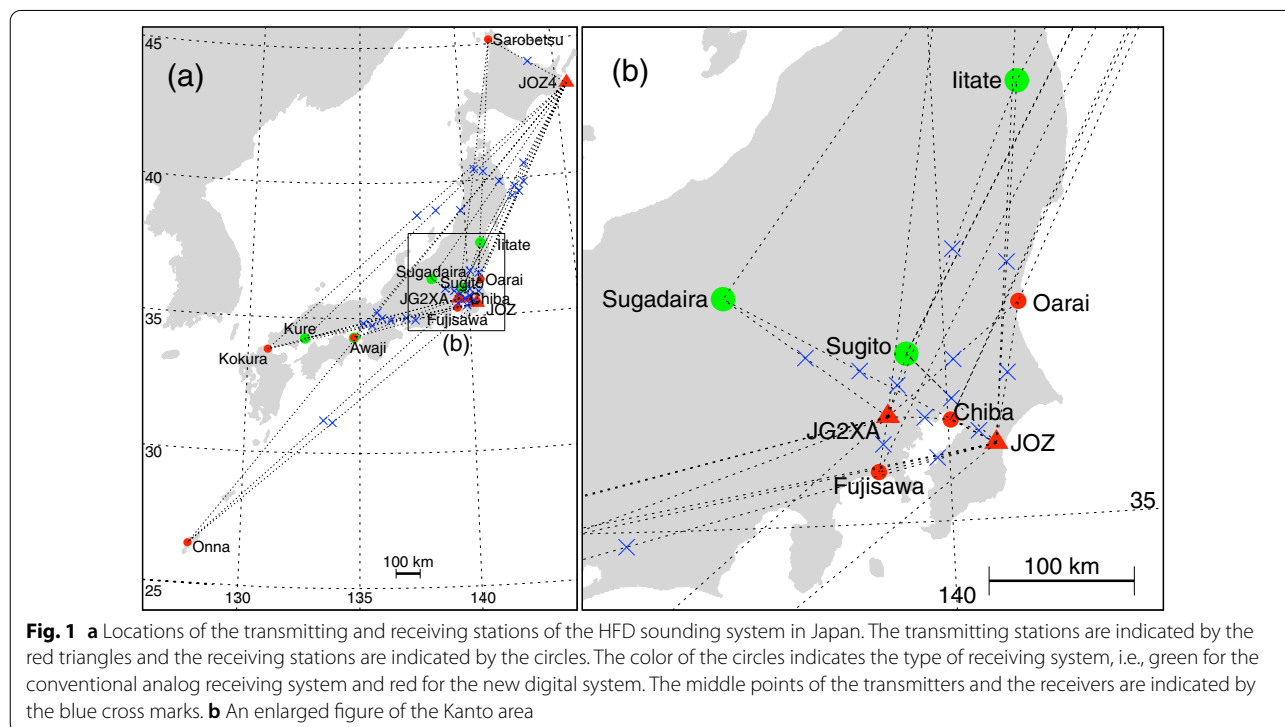
Nakata *et al. Earth, Planets and Space*   (2021) 73:209

Page 5 of 16

Table 1 Transmitters used for HFD observation

Frequency	Call sign	Location of transmitter	Power
5006 kHz	JG2XA	Chofu Campus of UEC, Tokyo	200 W
8006 kHz			
6055 kHz	JOZ2	Nagara, Chiba	50 kW
9595 kHz (- Sep., 2018)	JOZ3		
3925 kHz (Mar., 2020 -)	JOZ4	Nemuro, Hokkaido	10 kW

broadcasting Radio NIKKEI (35.465N, 140.359E) with the call sign JOZ2 and JOZ3, respectively, which are not always operational throughout the day. The radio wave at 9595 kHz was terminated on 30 September 2018. In the new digital receiving system, public broadcaster JOZ4 transmitting at a frequency of 3925 kHz from Nemuro, Hokkaido (43.297N, 145.563E) with a power of 10 kW was selected as a new target radio wave. The list of

Table 2 Receiving stations as of March 2021

Station	ID	Analog/ Digital	Lat (N)	Lon (E)	Distance from Tx (km)		
					JG2XA (Chofu)	JOZ2/JOZ3 (Nagara)	JOZ4 (Nemuro)
Sarobetsu	SAR	Digital	45.162	141.754	1072.2	1083.7	367.4
Iitate	IIT	Digital	37.689	140.673	247.1	248.7	747.4
Sugadaira	SGD	Analog	36.423	138.318	139.1	212.2	981.7
Oarai	ORI	Digital	36.331	140.587	120.0	98.4	882.6
Sugito	SGT	Analog	36.042	139.708	45.2	86.9	948.5
Chiba	CHB	Digital	35.629	140.104	50.7	29.4	971.8
Fujisawa	FJS	Digital	35.320	139.457	38.3	83.3	1029.6
Awaji	AWJ	Both	34.293	134.736	463.2	528.8	1369.0
Kure	KUR	Analog	34.243	132.529	657.8	726.6	1509.2
Kokura	KOK	Digital	33.816	130.872	817.6	886.1	1650.9
Onna	ONA	Digital	26.499	127.845	1506.3	1551.3	2457.5

Fig. 1 **a** Locations of the transmitting and receiving stations of the HFD sounding system in Japan. The transmitting stations are indicated by the red triangles and the receiving stations are indicated by the circles. The color of the circles indicates the type of receiving system, i.e., green for the conventional analog receiving system and red for the new digital system. The middle points of the transmitters and the receivers are indicated by the blue cross marks. **b** An enlarged figure of the Kanto area

Nakata *et al. Earth, Planets and Space*   (2021) 73:209

Page 6 of 16

receiving stations utilizing both analog and digital systems in the present system is given in Table 2. Figure 1 shows the locations of transmitters and receivers. The transmitters and analog/digital receivers are denoted in the figure by red triangles and green/red circles, respectively. The blue crosses denote the mid-points between the transmitter and receivers, at which the radio waves are assumed to be reflected.

Conventional analog receiving system

Radio waves arriving at remote sites were received by a 1 m diameter loop antenna (Wellbrook Communications ALA-1530) directed to the JG2XA transmitting station. A pre-amplifier was installed at the base of the antenna to amplify the received signal. The analog receiving system consists of single superheterodyne receivers for the corresponding frequencies of 5006, 6055, 8006, and 9595 kHz, as shown in Fig. 2. The received radio signal is down-converted to a baseband signal, and the AD-converted signal intensity is finally recorded as electric field strength [V/m]. The dynamic spectrum of the signal is obtained by applying the fast Fourier transform (FFT) to the time series of the raw electric field strength. The frequency with the largest signal amplitude at a certain time was derived as the Doppler frequency. Because the received raw signal intensity in the analog receiver is not complex but is a real signal, the Doppler spectrum shows a symmetrical spectral distribution centered at 0 Hz when the FFT is applied. This makes it impossible to distinguish between the positive and negative Doppler frequencies. To distinguish between positive and negative Doppler frequencies, the frequency is deliberately shifted by 8 Hz when down-converting the received radio waves. For example, a direct digital synthesizer (DDS) in a unit receiving the 5006 kHz radio wave provides a signal at a frequency of 5,005,992 Hz. This means that the analog

receiving system can observe the Doppler frequencies from -8 Hz to 8 Hz. The specific distribution of spectral intensity will be discussed later. Local frequencies, shifted by 8 Hz from the observation frequencies, were generated by direct digital synthesizers stabilized by an Rb frequency reference at a frequency of 10 MHz. The baseband signals go through second-order active low-pass filters (cutoff: 17 Hz) and high-pass filters (cutoff: 0.5 Hz) before the analog/digital (A/D) conversion. High-pass filters are necessary because the DC component of the baseband signals causes interference in the receiving system. After filtering, the baseband signals were sampled by an A/D converter with 16-bit integer values at a sampling rate of 100 Hz. The time accuracy of the data is determined by a PC whose time is synchronized using the network time protocol. The time synchronization accuracy has been set to be less than 10 ms. All the data obtained at the remote sites are transferred to the central data archive server at the UEC through the Internet. The Doppler frequencies are then calculated at the server-side every 10 s by applying the FFT to 4096 samples in approximately 40 s time window. Quick look (QL) plots of the derived Doppler frequencies and dynamic spectra of the raw data (termed the f-t diagram) are provided in near real-time at the website of the project (http://gwave. cei.uec.ac.jp/~hfd/plt.html).

New digital observation system

We have developed a new digital receiving system equipped with a commercially available SDR device (Ettus Research USRP N210). An LFRX daughterboard, which is a circuit board developed for USRP to receive signals between 0 to 30 MHz, is incorporated in model N210 to receive radio waves in the HF band together with the GPS-disciplined oscillator (GPSDO) for a 10 MHz reference signal. In the N200 series of USRP, signal processing that included modulation and demodulation was performed on the PC side. The data segments were transferred to the host PC through a local area network.

The USRP operation can be performed using the GNU Radio free software. Using the software libraries, we created a radio by connecting signal processing packages. A user can easily build a radio by connecting the inputs and outputs of multiple blocks. Such a connection can be made using the GNU Radio Companion GUI software, which allows the system to be graphically configured inside the USRP. Figure 3 provides a flow graph used for the HFD observations made by the GNU Radio Companion. The observation procedure of the new receiver is basically the same as that of the analog receivers. In the current system, the received signal flows into four block groups for each frequency (3925, 5006, 6055, and 8006 kHz) from the source (the signal from the antenna).
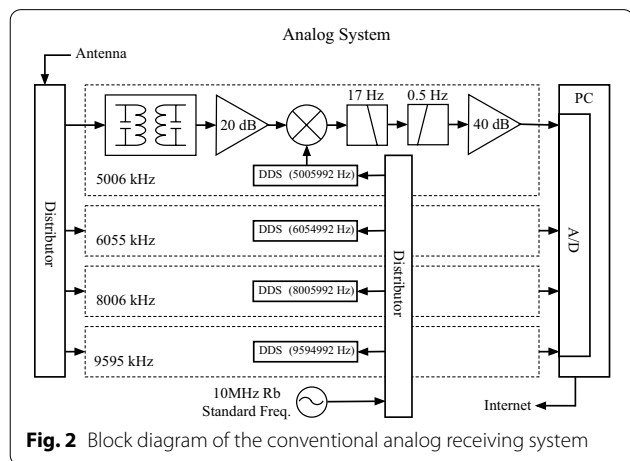

Fig. 2 Block diagram of the conventional analog receiving system

Nakata *et al. Earth, Planets and Space* (2021) 73:209
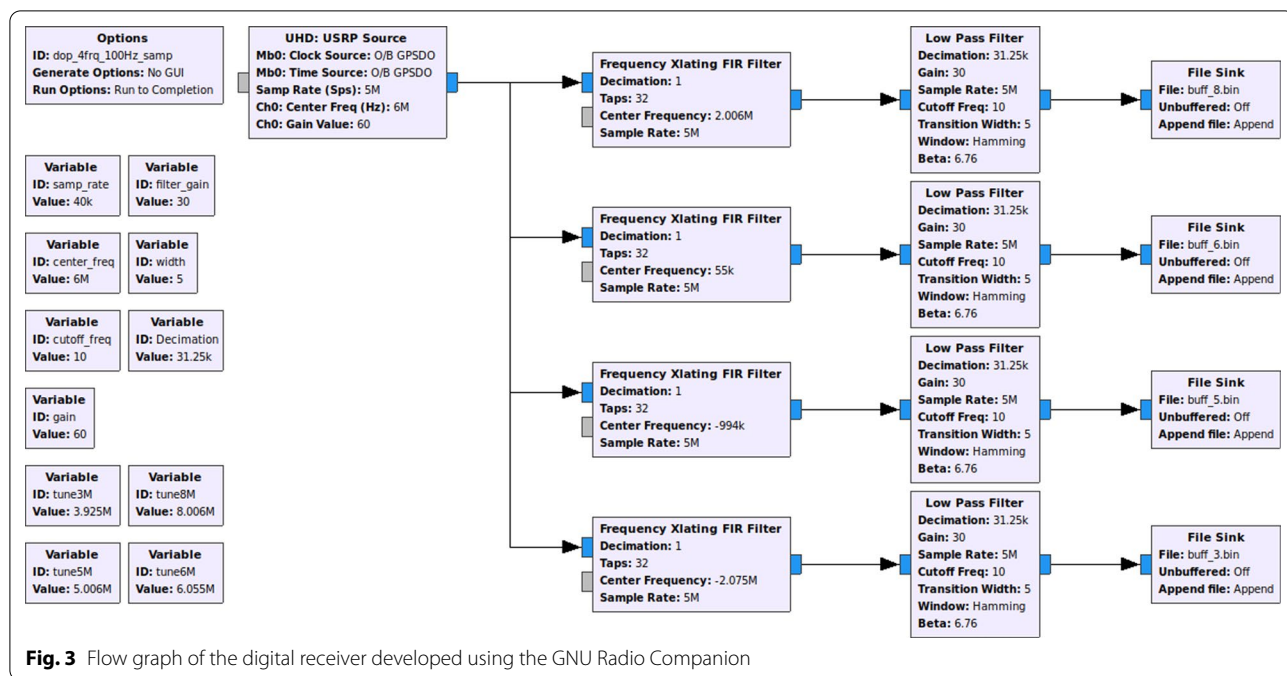
Page 7 of 16

Fig. 3 Flow graph of the digital receiver developed using the GNU Radio Companion

The USRP receives signals from the antenna with a center frequency of 6 MHz at a sampling frequency of 5 MHz in the "UHD: USRP Source" block. Therefore, the system can capture signals with a range of ± 2.5 MHz (i.e., 3.5 MHz to 8.5 MHz). Each frequency multiplying finite impulse response (FIR) filter shifts the signal to the desired frequency in the "Frequency Xlating FIR Filter" block. The "Low-Pass Filter" block passes the signals within the ± 10 Hz band centered at the carrier frequency and decimate signals to 100 Hz sampling. The signals are stored in the "File Sink" block. The procedure from the frequency multiplying FIR filter is executed on the PC side. The signal processing flow is illustrated schematically in Fig. 4. Because the USRP captures signals as in-phase and quadrature-phase (IQ) values, positive and negative Doppler frequencies can be distinguished using FFT. The signal intensities of the carrier frequencies can thus be captured directly by the digital receiver. The properties of both systems are listed in Table 3.

Cross-evaluation of analog and digital receivers

Prior to the actual observation, we evaluated the performance of the new digital receiver. A schematic illustration of the evaluation system is shown in Fig. 5. A GPS-disciplined monochromatic signal at a frequency of 8006 kHz was used as a signal input of the antenna coupler so that the same signals were supplied to both the analog and digital receivers simultaneously. The output levels of both receivers are shown in Fig. 6a. We examined the variations in the gains of both systems for the
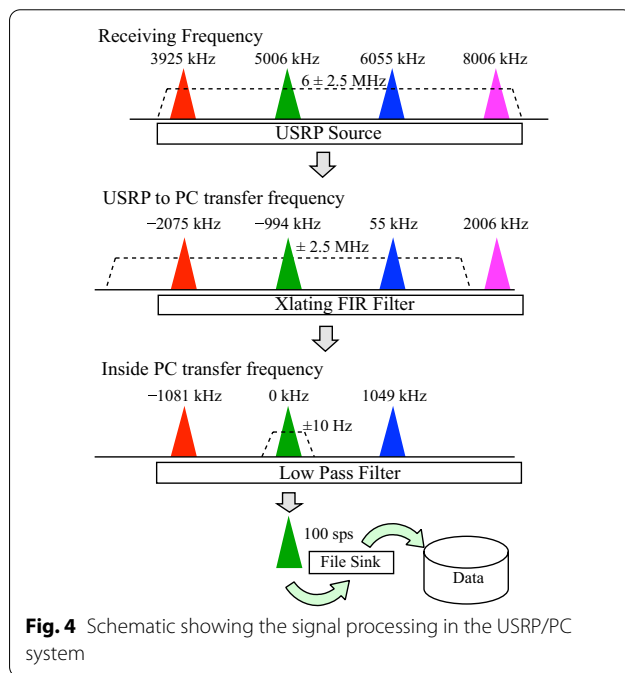
Fig. 4 Schematic showing the signal processing in the USRP/PC system

same input signal intensity because these output values are delivered by a built-in software whose internal processing coefficients are not available. The black line in Fig. 6a shows the output variation of an ideal linear response. In both systems, the output level varied linearly with respect to the input level, indicating the possibility to observe the power variations according to the

Nakata *et al. Earth, Planets and Space*   (2021) 73:209

Page 8 of 16

Table 3 The comparison of the specifications of the analog system with those of the digital system

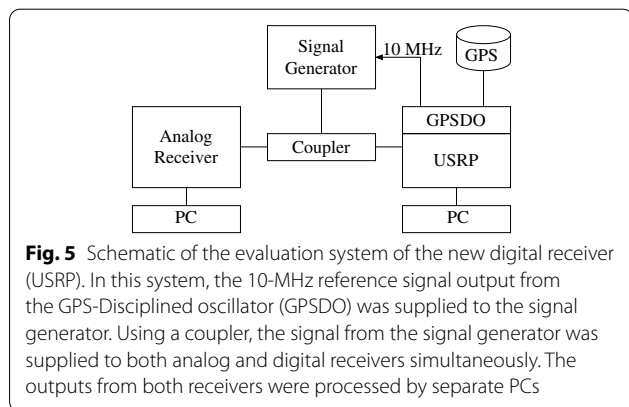|	Analog system	Digital system
Channel	4	4
Reference Frequency	Rb Frequency Standard	Build in GPS receiver
System	Direct frequency conversion then A/D	A/D then multiple direct frequency conversion
Detection	8 Hz frequency offset detection	IQ coherent detection
Filtering	Active LPF and HPF	Digital LPF
Sampling	16 bit 100 sps (at the receiver output)	14 bit IQ 100 Msps (at the receiver input)

Fig. 5 Schematic of the evaluation system of the new digital receiver (USRP). In this system, the 10-MHz reference signal output from the GPS-Disciplined oscillator (GPSDO) was supplied to the signal generator. Using a coupler, the signal from the signal generator was supplied to both analog and digital receivers simultaneously. The outputs from both receivers were processed by separate PCs
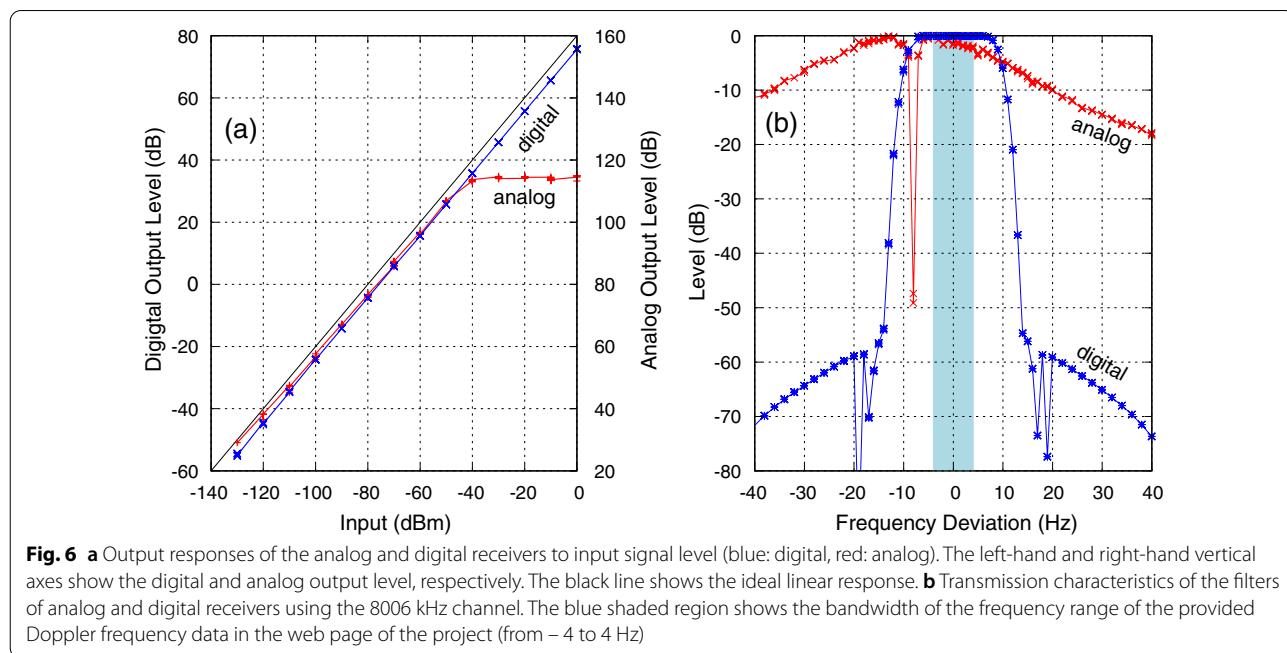
reception power of the radio waves. In the analog system, however, the output level slightly deviated from the linear response when the input was weaker than -100 dBm. Concerning the dynamic range, the output level of the analog receiver was saturated at an input level of -40 dBm, while the digital receiver responded linearly to 0 dBm. The findings indicated that the dynamic range of the digital receiver is larger than 130 dB. Such a wide dynamic range is achieved using oversampling technique. For an ideal N-bit AC converter, the signal-to-noise ratio (SNR) can be expressed as

$$\text{SNR} = 6.02N + 1.76 + 10\log_{10}\left(\frac{f_s}{2 \times \text{BW}}\right)[\text{dB}], \quad (7)$$

where f_s is the sampling frequency and BW is the signal bandwidth (Kester, 2005). In our system, the sampling frequency was 5 MHz, and the bandwidth was ± 10 Hz, namely 20 Hz. As a result, the total SNR was 137.4 dB. This indicated that the digital receiver is capable of handling observations with a wide dynamic range.

Next, we examined the filtering characteristics of both receivers for the baseband signal. In this examination, the test signal at a frequency of 8006 kHz was input to both receivers by shifting the frequency of the test signal from -40 to $+40$ Hz. The results are presented in Fig. 6b. In the usual observation, the Doppler frequency is derived within the range of ± 4 Hz (a light-blue shaded area), as shown in the Quick-Look (QL) of the project

Fig. 6 a Output responses of the analog and digital receivers to input signal level (blue: digital, red: analog). The left-hand and right-hand vertical axes show the digital and analog output level, respectively. The black line shows the ideal linear response. **b** Transmission characteristics of the filters of analog and digital receivers using the 8006 kHz channel. The blue shaded region shows the bandwidth of the frequency range of the provided Doppler frequency data in the web page of the project (from − 4 to 4 Hz)

Nakata *et al. Earth, Planets and Space*   (2021) 73:209

Page 9 of 16

website. The second-order high-pass and low-pass filters incorporated in the analog circuit have broad filter characteristics. However, the digital system has steep shoulder characteristics because the signals are processed numerically. This leads to a reduction in the unwanted contribution from noise and interference of the digital system. We discuss this point later in this paper. The level of the analog receiver is shown in the red line of Fig. 6b and has a dip at −8 Hz because the DC component of the baseband signal is cut by the second-order active high pass filter (cutoff: 0.5 Hz) shown in Fig. 2.

Figure 7 shows the spectra of both the digital and analog receivers. To obtain these data, a test signal at a frequency of 5006 kHz was input to both receivers by changing the frequency of the test signal from −40 to +40 Hz. The rectangles located in the center of Fig. 7a, b indicate the frequency range of the QL (from −4 to +4 Hz). The output signal at a frequency of −8 Hz in Fig. 7a is a leakage of the local oscillator signal from the analog receiver because this signal appeared only when both the analog and digital receivers were connected through a coupler as shown in Fig. 5. In a digital system, the frequency of the output signal varies corresponding to the frequency of the input signal. The output outside ±10 Hz is suppressed due to the low-pass filter with steep shoulder characteristics, as described previously. On the other hand, in the analog system, a mirror-image output symmetrical to −8 Hz appeared to be caused by the FFT signal processing. Noise signals with fluctuating frequencies also appeared in the output frequencies below −30 Hz and above 10 Hz. The noise was also

suppressed in the digital system owing to the better characteristics of the low-pass filter.

Pilot observations

Side-by-side comparison between analog and digital receivers

As described in the previous section, the digital receiver has sufficient performance for actual Doppler observations. Accordingly, we commenced actual test of Doppler observations using both analog and digital receivers located at the Minami-Awaji Shichi Campus of Kibi International University (AWJ). The location of the AWJ station is shown in Fig. 1a. The ground distances from the AWJ station to the transmitters are 463 km for JG2XA and 528 km for JOZ. Thus, only the sky waves, which are reflected in the ionosphere, are received, and the ground wave can be neglected in the observation at AWJ. As shown in Fig. 8, both receivers are installed onsite. We recognize that the size of the digital receiver becomes quite small compared to the analog receiver. The signals received by the loop antenna are fed to both systems simultaneously through the antenna coupler. The data obtained from the two systems were processed through a common procedure involving the sampling rate, FFT, and other aspects, and thus could be directly compared.

Figure 9 depicts the dynamic spectrum from both systems at a frequency of 5006 kHz on 18 January 2021. On this day, the radio wave was received with relatively strong signal intensity during the daytime (8–21 JST). The Doppler frequency was determined for both

Fig. 7 Dynamic spectra obtained with **a** the digital receiver and **b** the analog receiver. The plot shows the response to input frequency in the range from − 40 to + 40 Hz with respect to the center frequency of 5006 kHz

Nakata *et al. Earth, Planets and Space*   (2021) 73:209

Page 10 of 16
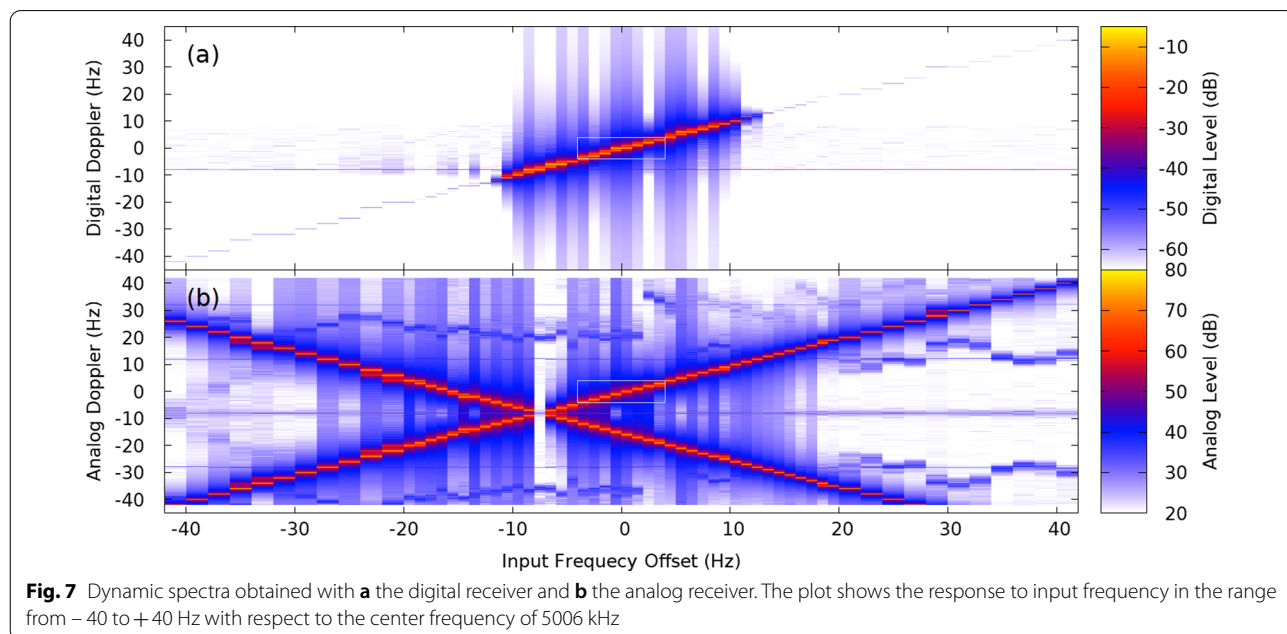
systems. However, the analog system suffered considerable noise throughout the day and showed apparent contamination, as shown in Fig. 9b. Because the digital system provides sharp filtering to the baseband signal, as shown in the section of cross-evaluation of analog and digital receivers, the digital system eliminates background noise. Figure 9c, d display the received signal intensity versus the Doppler frequency at 12 JST. These figures correspond to the cross-sections at 12 JST in

Fig. 9a, b, respectively. As seen in Fig. 9a, b, the background noise was significantly attenuated in the digital receiver. Figure 9c also shows that the noise in the digital receiver is strongly suppressed compared to the analog receiver. The superposition of Fig. 9c, d is shown in Fig. 10. The signal-to-noise ratio of the analog receiver was approximately 10 to 20 dB, while that of the digital receiver reached 40 dB. These findings indicate the improvement of the signal-to-noise ratio in the digital system by more than 20 dB compared to the analog in actual observations.

Case examples
The results presented in the previous subsection support the conclusion that the digital receivers are suitable for actual Doppler observations. Therefore, we replaced several analog receivers in our observation system with digital receivers. Here, we show two examples of actual HFD observations to demonstrate the ability of digital receivers to measure ionospheric perturbations.

Observations of MSTID during daytime in winter
At mid-latitudes, medium-scale traveling ionospheric disturbances (MSTIDs) are usually observed during daytime in winter and during nighttime in summer (Hunsucker 1982). Here, we introduce an MSTID event
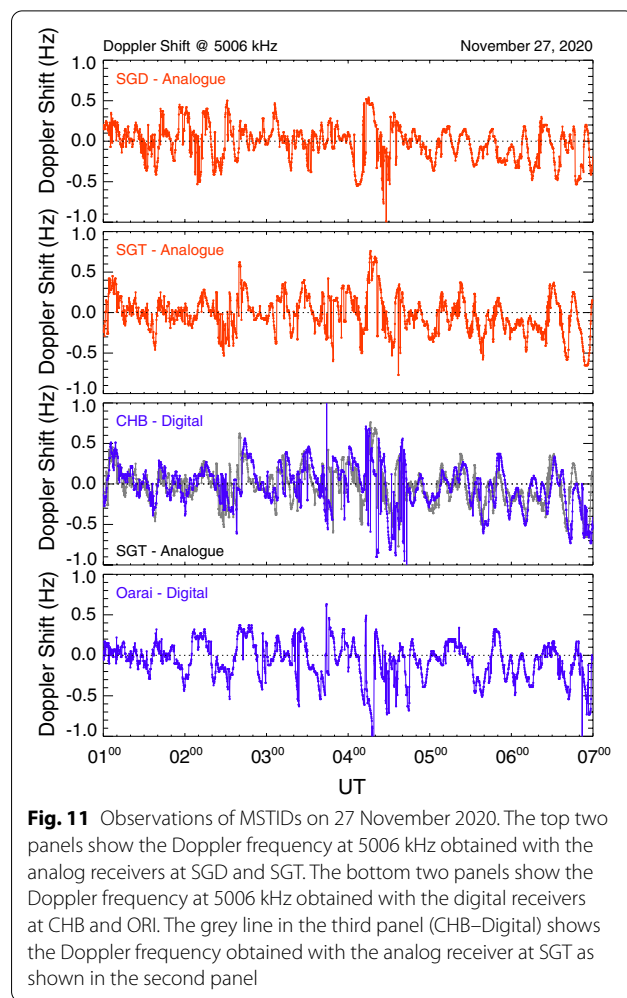

Fig. 8 Photo of the digital (top side) and analog (bottom side) receiving systems in Awaji
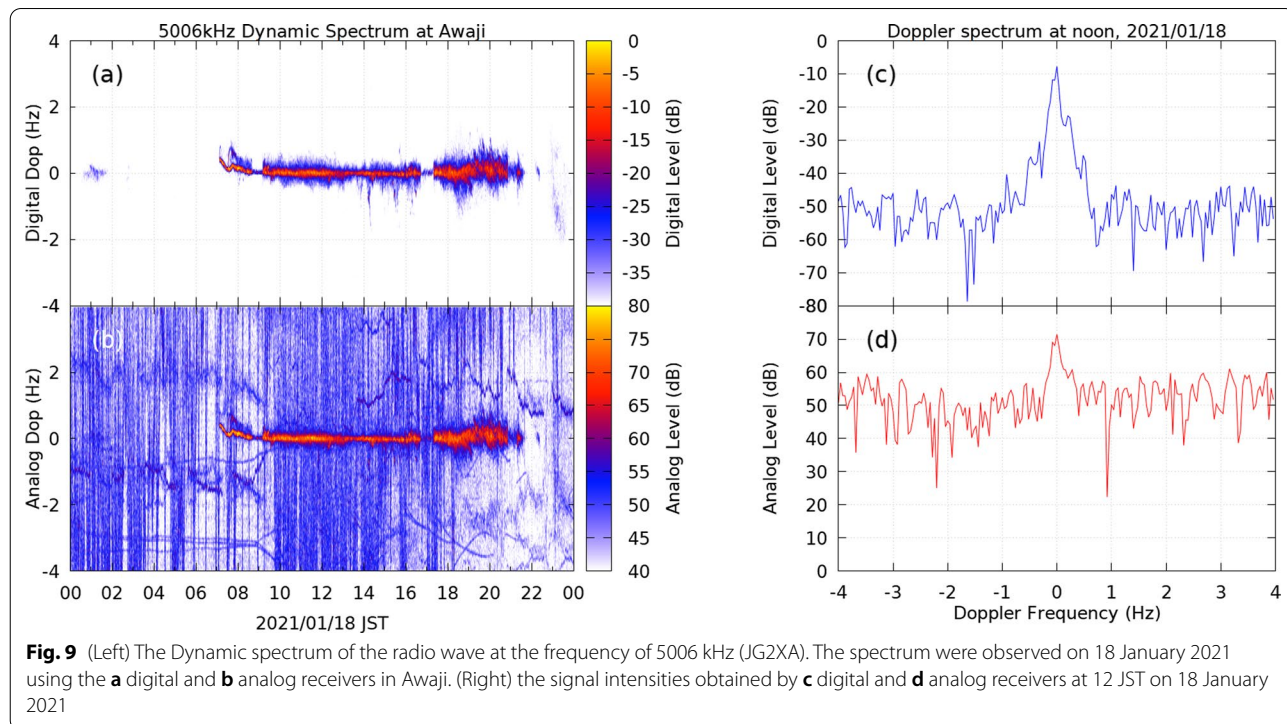
Fig. 9 (Left) The Dynamic spectrum of the radio wave at the frequency of 5006 kHz (JG2XA). The spectrum were observed on 18 January 2021 using the **a** digital and **b** analog receivers in Awaji. (Right) the signal intensities obtained by **c** digital and **d** analog receivers at 12 JST on 18 January 2021

Fig. 10 The plot superposed to the data shown in Fig. 9c, d
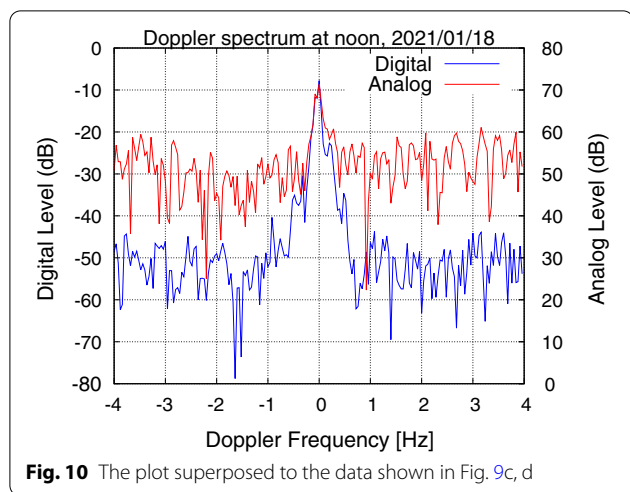
during daytime in winter, which was obtained on 27 November 2020. Figure 11 shows the 5006 kHz Doppler frequency data from four stations in the vicinity of the transmitter (Sugadaira, Sugito, Chiba, and Oarai; see Fig. 1b for the detailed location of these stations). Because the reflection points between these stations and the 5006 kHz transmitter (JG2XA) at UEC are close to each other, the Doppler frequency data show very similar wavy features throughout the interval. The features correspond to the variations in altitude of the reflection points induced by the passage of MSTIDs across the sensing area. The receiving systems at Oarai and Chiba are newly developed digital receivers, and those at Sugito and Sugadaira are conventional analog receivers. In the third panel from the top, we plot the digital and analog data from Chiba (blue) and Sugito (gray), whose reflection points were very close (approximately 30 km separation). This direct comparison demonstrates that the Doppler frequency variations from the new system are very similar to those from Sugito. The findings confirmed the feasibility of using the USRP-based system for the digital receiver.

The observations shown in Fig. 11 were obtained during the daytime. Thus, the signatures of MSTIDs are manifestations of AGWs in winter (Shibata and Okuzawa 1983; Shibata 1986). Recently, Chum et al. (2021) employed multi-point and multi-frequency HFD observations in the Czech Republic to derive the three-dimensional propagation of AGWs at thermospheric/ionospheric altitudes. The HFD observation network in Japan, which partially includes newly developed digital receivers, can also be used to estimate the propagation characteristics, possibly in three dimensions, because most of the Rx stations record signals at four different frequencies reflected at different altitudes. While the

Fig. 11 Observations of MSTIDs on 27 November 2020. The top two panels show the Doppler frequency at 5006 kHz obtained with the analog receivers at SGD and SGT. The bottom two panels show the Doppler frequency at 5006 kHz obtained with the digital receivers at CHB and ORI. The grey line in the third panel (CHB–Digital) shows the Doppler frequency obtained with the analog receiver at SGT as shown in the second panel

details are not provided in this paper, the newly developed digital receivers were also able to detect the signatures of MSTIDs during the night in the summer months. These signals were produced by the plasma instability in the electric coupling between the *E* and *F* regions of the ionosphere (Otsuka et al. 2007; Yokoyama et al. 2009). The multi-point HFD observations, which will be enabled by the development of the digital receiver, will allow us to investigate the propagation characteristics of such MSTIDs in both winter and summer.

Psc event observed simultaneously with magnetometer data

Changes in the Interplanetary Magnetic Field (IMF) and dynamic pressure of the solar wind cause magnetospheric disturbances such as geomagnetic storms, substorms, magnetic SCs, and geomagnetic pulsations (Pc). The electric fields generated by the magnetospheric disturbances propagate to the polar ionosphere via field-aligned currents and propagate almost instantaneously to the global

Nakata *et al. Earth, Planets and Space* (2021) 73:209

Page 12 of 16

ionosphere in the earth-ionosphere waveguide (Kikuchi and Araki 1979; Kikuchi et al. 1996). The propagated electric fields cause the ionospheric plasma to move perpendicular to the magnetic field lines owing to the ExB drift. As a result, the altitude of the reflection point of the HF radio wave changes. Thus, the electric field strength can be estimated from the Doppler frequency obtained with the HFD sounding system, as has been done for the SC (Davies et al. 1962; Kikuchi et al. 1985, 2016, 2021; Sastri et al. 1993), Pc5, and Pi2 geomagnetic pulsations (Baddeley et al. 2005; Motoba et al. 2004; Reddy et al. 1994), quasiperiodic DP2 magnetic fluctuations (Abdu et al. 1998; Sastri et al. 2000), substorms (Tsutsui et al. 1988; Hashimoto et al. 2017), and geomagnetic storms (Hashimoto et al. 2020).

Figure 12(a) shows the Pc5 magnetic oscillations observed at the Kakioka magnetic observatory (KAK: 36.2N, 140.2E in geographic coordinate, 28.0N in magnetic latitude) in Japan during an SC that began at 1058 UT (1958 MLT) on 16 September 2020. This Pc5 event featured damped oscillations with a period of approximately 9 min, which can be classified as Psc5 (Kato and Saito 1958). During Psc5, periodic oscillations in the HFD frequency were observed by both the analog and digital receivers in AWJ (Fig. 12b), indicating that the motion of the ionosphere is caused by the electric field of the Psc5 with the intensity up to 1.73 mV/m. Figure 12a also shows that the Psc5 was observed at the daytime low latitude, Kourou in French Guiana (KOU: 5.2N, 52.7 W in geographic coordinate, 14.0N in magnetic latitude) and at the daytime magnetic equator, Huancayo in Peru (HUA: 12.1 S, 75.3 W in geographic coordinate, 2.6S in magnetic latitude).

As shown by the vertical dotted lines in Fig. 12, the oscillations in the Doppler frequency were out of phase with those in the Psc5 at KAK located near the HF Doppler observations. However, the Doppler frequency was in phase with the equatorial electrojet (EEJ) on the dayside, as determined by subtracting X(KOU) from X(HUA). The correlation between the nighttime Doppler frequency and daytime EEJ is in accordance with the results of Motoba et al. (2004), which showed that the oscillations of the Doppler frequency at low latitudes are due to ExB drifts caused by the direct penetration of the polar electric field. The correlation between the Doppler frequency and the EEJ has been observed during the SC (Kikuchi et al., 2021), DP2 fluctuations (Abdu et al., 1998) and substorms (Hashimoto et al., 2017), which supports the idea that the Doppler frequency at AWJ (Fig. 12b) is associated with the global ionospheric currents of the Psc5. On the other hand, the Psc5 observed at KAK and KOU were not caused by the ionospheric currents driven by the ionospheric electric field, but rather by
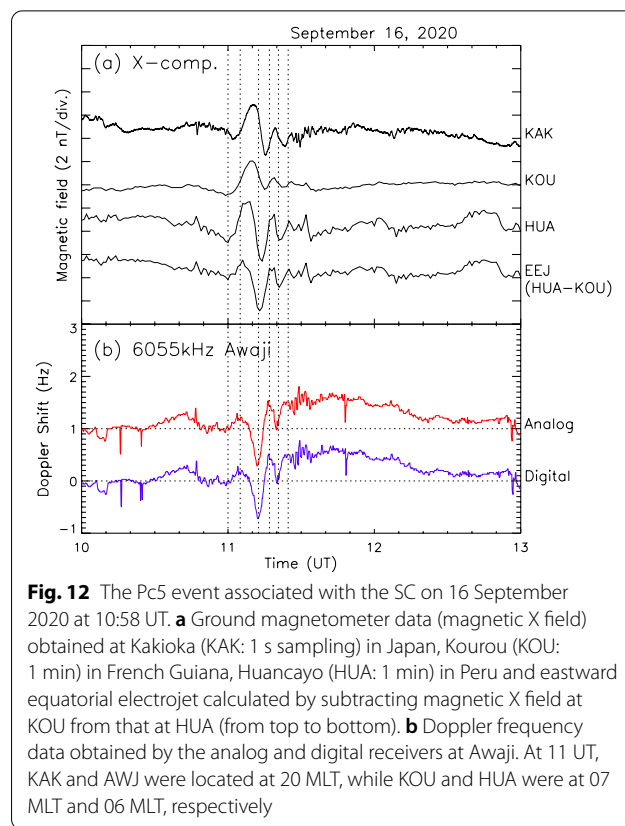

Fig. 12 The Pc5 event associated with the SC on 16 September 2020 at 10:58 UT. **a** Ground magnetometer data (magnetic X field) obtained at Kakioka (KAK: 1 s sampling) in Japan, Kourou (KOU: 1 min) in French Guiana, Huancayo (HUA: 1 min) in Peru and eastward equatorial electrojet calculated by subtracting magnetic X field at KOU from that at HUA (from top to bottom). **b** Doppler frequency data obtained by the analog and digital receivers at Awaji. At 11 UT, KAK and AWJ were located at 20 MLT, while KOU and HUA were at 07 MLT and 06 MLT, respectively

magnetospheric currents, such as magnetopause currents and field-aligned currents (Kikuchi and Hashimoto 2016).

The Doppler shifts of the new digital receiver agree well with those of the analog receiver in terms of time evolution and amplitude. Because the digital receiver is simple and inexpensive, the new receiving system makes it easy to deploy receiving points overseas and maintain continuous operation. Electric fields that originate from the magnetosphere can be observed simultaneously on a global scale. The global deployment of the new system would enable the observation of the electric fields originating from the magnetosphere in the global ionosphere. The new system would contribute to the research of the mid- and low-latitude ionosphere, in particular, coupling from the polar ionosphere and magnetosphere.

Discussion

In this paper, we introduce a new digital receiving system for HFD observations in Japan. We also provide several case examples of actual observations obtained with the new digital receivers in comparison with those from the conventional analog receivers. There are several advantages of the new digital system:

Nakata *et al. Earth, Planets and Space*   (2021) 73:209

Page 13 of 16

1. The system has a wide dynamic range compared with the analog system, which enables the detection of weak signatures of ionospheric reflection.
2. The Doppler spectrum from the digital system is free from image contamination in the FFT process using IQ coherent detection.
3. The shoulder characteristics of the frequency response are improved by the use of digital filters, which reduces interference.
4. There is no need to assemble an analog circuit to produce the receiving system. The digital system can be prepared without any knowledge of analog devices, which makes it much easier to reproduce the system and install the receivers into multiple stations. It is easy to construct a receiving system by connecting only the blocks of each specific function on the GUI flow graph.
5. The digital system is much smaller and less expensive than the conventional analog receiver, which contributes to expanding the network observations in the framework of the distributed array of small instruments.
6. Even if other radio waves are received, or the transmission system is changed in the future, it can be

easily handled by simply changing the process in the flow graph.

The frequencies of the JG2XA transmitters and receivers are referenced to 10 MHz signals from the Rb and GPSDO frequency standards, respectively, whose frequency accuracies are on the order of 10^{-11}. Therefore, it is expected that the accuracy of the Doppler frequency determined by the digital receiving system is less than 1 mHz. To check this, we examined the Doppler frequency obtained at several digital receiving points, as shown in Fig. 13. To obtain this data, the FFT was performed using a time series of 1000 s duration. Thus, the Doppler frequency was derived with a frequency resolution of 1 mHz. These Doppler frequency values were sampled at approximately 03 UT (12 JST). At this time, the propagation of the radio waves should be stable and the Doppler frequency should be minimal. In Fig. 13, the Doppler frequency for 5006 kHz and 8006 kHz is indicated in red and green, respectively. Because the distance between AWJ and JG2XA is longer than the distance between AWJ and CHB/FJS, the Doppler frequency at AWJ fluctuates more than at CHB and FJS. Only sky waves are received in the path between JG2XA and AWJ, while ground waves are
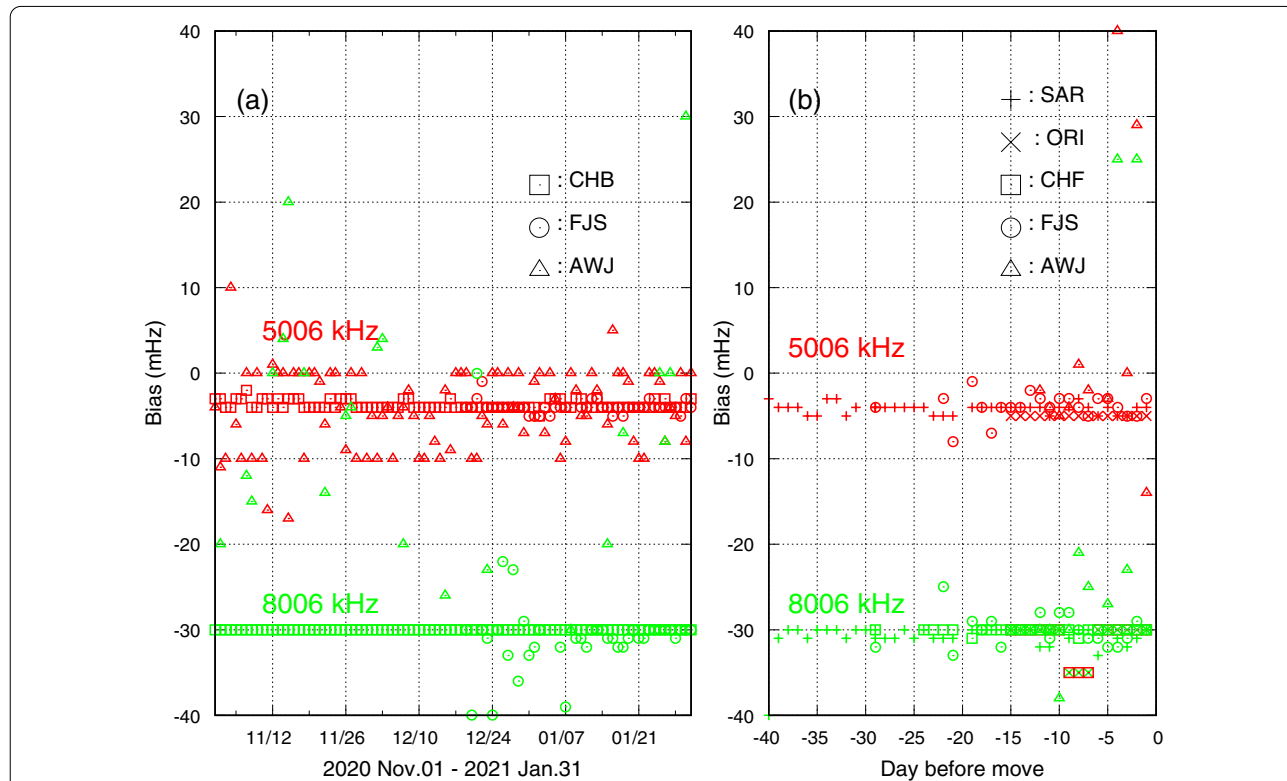
Fig. 13 Frequency bias in Doppler frequency. **a** Doppler frequency obtained at three digital receiving stations (CHB, FJS, and AWJ), which were sampled at 03 UT (12 JST) for two months from 01 November 2020 to 31 January 2021. **b** Doppler frequency obtained by the receivers under a receiving test in the laboratory for deployment to five stations (SAR, ORI, CHF, FJS, and KOK)

Nakata *et al. Earth, Planets and Space*   (2021) 73:209

Page 14 of 16

received together with sky waves in CHB and FJS. The frequency biases for 5006 kHz and 8006 kHz were approximately 3 mHz and 30 mHz, respectively, regardless of the location of the Rx stations (Fig. 13a). Most of the receiving systems were tested at the laboratory within a distance of 100 m from the JG2XA transmitting antenna in the Chofu Campus (CHF) before deployment to the remote site. Figure 13b shows the fine Doppler shifts obtained at CHF. The format was the same as that in Fig. 13a. The Doppler shift values again demonstrated the existence of identical biases. Furthermore, we checked whether this Doppler shift was due to the difference in frequency accuracy between the transmitter and receiver. To do so, signals at frequencies of 5006 kHz and 8006 kHz from the function generator, referenced to the GPSDO incorporated in the USRP receiver, were input to the digital receivers. Although the Doppler frequency should be zero in this experiment, the frequency bias, as shown in Fig. 13, still appeared. Therefore, the biases in the Doppler frequency seem to be attributed to the frequency references used in the transmitters/receivers and also to the data processing in the A/D sampling, frequency conversion, and decimation processes incorporated within the USRP/PC system. However, this frequency shift can be treated as unaffected when using the data obtained by this digital system. As shown in Figs. 11 and 12, most of the actual ionospheric phenomena displayed frequency variations of several onetenth Hz to several Hz. The observed biases (3 mHz for 5006 kHz and 30 mHz for 8006 kHz) corresponded to the vertical motion of the ionosphere of less than 1 m/s, indicating that the biases were too small to affect the observations. Moreover, in most events, a relative temporal variation of the Doppler shift was used. Thus, the small biases near the zero-Doppler level did not directly influence the observations. In the normal data production process, we employed an FFT window of 40-s duration, and the corresponding frequency resolution was 25 mHz. Hence, the frequency biases that appear in our digital receiving system are sufficiently small to be ignored in typical scientific cases.

In this paper, we describe the fundamental characteristics of the new digital system for HFD observations in Japan. We installed the new system in seven Rx sites (as of May 2021) out of a total of 11 Rx stations. We plan to deploy digital receivers in the remaining four stations by the end of 2021 to complete networked HFD observations with digital receivers. We also plan to modify the Tx station using a new digital-based transmission system. In the new Tx system, FMCW-based coding is added to the existing CW wave to enable the range measurement of the propagation path between the Tx and Rx stations. With this ranging capability, we can estimate the altitude of reflection, which further allows us to track the propagation

of acoustic waves from extreme atmospheric phenomena (e.g., earthquakes) without any ionospheric models. In addition, it will be possible to distinguish the reflections from the *E* and *F* regions, especially the reflection from sporadic E at an altitude of approximately 100 km and wavy phenomena (e.g., MSTIDs) in the *F* region. This contributes to a better understanding of the electric coupling process in the ionosphere (Cosgrove 2013).

Summary

We introduce a newly developed digital receiver for HFD observation using USRP. Comparison with the previous analog receiver reveals that the digital receiver has a very wide dynamic range and improvement in the high signal-to-noise ratio (> 20 dB). No major differences were observed in the measured Doppler frequency variations from the digital and analog systems during ionospheric wave structures and geomagnetic pulsations. Although there are small frequency biases, probably due to the internal signal processing within the combined USRP/PC system, these biases are sufficiently small compared to the typical Doppler frequency variations of ionospheric/magnetospheric origin. The advantages of the digital Rx system include: (1) flexible change in the signal reception (frequency, bandwidth, etc.) by replacing the software, (2) easy reproduction of the Rx system by copying the software without manufacturing analog circuits, and (3) much smaller equipment and relatively lower preparation cost. The analog receivers currently in operation will be soon replaced by new digital receivers.

Nakata *et al. Earth, Planets and Space*   (2021) 73:209

Page 15 of 16

Availability of data and materials

Data of the HFD sounding system in Japan and the source code for the receiver are both available at http://gwave.cei.uec.ac.jp/~hfd/. In association with the development of the new digital receiver, we are renewing the web page of HFD Sounding Experiment in Japan (http://gwave.cei.uec.ac.jp/~hfd/). This page displays QL plots of the HFD frequency and the intensity of the received radio wave. We also provide information on the HFD system and observation data (ASCII and binary data). The rule of the road for using HFD data is defined as shown in http://gwave.cei.uec.ac.jp/~hfd/rules-of-the-road_hfd.pdf. The magnetometer data from Kourou and Huancayo can be downloaded from INTERMAGNET website (https://www.intermagnet.org), and high time resolution data from Kakioka can be downloaded from Japan Meteorological Agency website (https://www.kakioka-jma.go.jp).

Declarations

Ethics approval and consent to participate
Not applicable.

Consent for publication
Not applicable.

Competing interests
The authors declare that they have no competing interests.

Author details
[1]Graduate School of Engineering, Chiba University, Chiba, Japan. [2]The University of Electro-Communications, Tokyo, Japan. [3]Kibi International University, Hyogo, Japan. [4]Institute for Space-Earth Environmental Research, Nagoya University, Aichi, Japan. [5]Center for Space Science and Radio Engineering, The University of Electro-Communications, Tokyo, Japan. [6]National Institute of Technology, Kitakyushu College, Fukuoka, Japan.

References

Abdu MA, Sastri JH, Luhr H, Tachihara H, Kitamura T, Trivedi NB, Sobral JHA (1998) DP 2 electric field fluctuations in the dusk-time dip equatorial ionosphere. Geophys Res Lett 25:1511–1514. https://doi.org/10.1029/98gl01096

Anderson S (2019) Cognitive HF radar. J Eng 2019:6772–6776. https://doi.org/10.1049/joe.2019.0537

Baddeley LJ, Yeoman TK, Wright DM (2005) HF doppler sounder measurements of the ionospheric signatures of small scale ULF waves. Ann Geophys 23:1807–1820. https://doi.org/10.5194/angeo-23-1807-2005

Bostan SM, Urbina JV, Mathews JD, Bilén SG, Breakall JK (2019) An HF software-defined radar to study the ionosphere. Radio Sci 54:839–849. https://doi.org/10.1029/2018rs006773

Bristow WA (2019) Application of RADAR imaging analysis to SuperDARN observations. Radio Sci. https://doi.org/10.1029/2019rs006851

Chisham G, Lester M, Milan SE, Freeman MP, Bristow WA, Grocott A, McWilliams KA, Ruohoniemi JM, Yeoman TK, Dyson PL, Greenwald RA, Kikuchi T, Pinnock M, Rash JPS, Sato N, Sofko GJ, Villain J-P, Walker ADM (2007) A decade of the Super Dual Auroral Radar Network (SuperDARN): scientific achievements, new techniques and future directions. Surv Geophys 28:33–109. https://doi.org/10.1007/s10712-007-9017-8

Chum J, Hruska F, Zednik J, Lastovicka J (2012) Ionospheric disturbances (infrasound waves) over the Czech Republic excited by the 2011 Tohoku earthquake. J Geophys Res 117:A08319. https://doi.org/10.1029/2012JA017767

Chum J, Liu JY, Laštovička J et al (2016) Ionospheric signatures of the April 25, 2015 Nepal earthquake and the relative role of compression and advection for Doppler sounding of infrasound in the ionosphere. Earth Planets Space 68:24. https://doi.org/10.1186/s40623-016-0401-9

Chum J, Podolská K, Rusz J, Baše J, Tedoradze N (2021) Statistical investigation of gravity wave characteristics in the ionosphere. Earth Planets Space 73:60. https://doi.org/10.1186/s40623-021-01379-3

Cosgrove R (2013) Mechanisms for E-F coupling and their manifestation. J Atmos Sol Terr Phys 103:56–65. https://doi.org/10.1016/j.jastp.2013.03.011

Davies K, Baker DM (1966) On Frequency variations of ionospherically propagated HF radio signals. Radio Sci. DOI: 10.1002/rds196615545

Davies K, Watts J, Zacharisen D (1962) A study of F2-layer effects as observed with a Doppler technique. J Geophys Res 67:2. DOI: 10.1029/JZ067i002p00601

Farges T, Le Pichon A, Blanc E, Perez S, Alcoverro B (2003) Response of the lower atmosphere and the ionosphere to the eclipse of August 11, 1999. J Atmos Sol Terr Phys 65:717–726. https://doi.org/10.1016/S1364-6826(03)00078-6

Greenwald RA, Baker KB, Dudeney JR, Pinnock M, Jones TB, Thomas EC, Villain J-P, Cerisier J-C, Senior C, Hanuise C, Hunsucker RD, Sofko G, Koehler J, Nielsen E, Pellinen R, Walker ADM, Sato N, Yamagishi H (1995) DARN/SuperDARN. Space Sci Rev 71:761–796. https://doi.org/10.1007/BF00751350

Guo Q, Zheng Y, Chernogor LF, Garmash KP, Rozumenko VT (2019) Passive HF Doppler radar for oblique-incidence ionospheric sounding. In: 2019 IEEE 2nd Ukraine Conference on Electrical and Computer Engineering (UKRCON). pp 88–93

Hashimoto KK, Kikuchi T, Tomizawa I, Nagatsuma T (2017) Substorm overshielding electric field at low latitude on the nightside as observed by the HF Doppler sounder and magnetometers. J Geophys Res 122:10851–10863. https://doi.org/10.1002/2017ja024329

Hashimoto KK, Kikuchi T, Tomizawa I, Hosokawa K, Chum J, Buresova D, Nose M, Koga K (2020) Penetration electric fields observed at middle and low latitudes during the 22 June 2015 geomagnetic storm. Earth Planets Space 72:71. https://doi.org/10.1186/s40623-020-01196-0

Ichinose T, Ogawa T (1974) HF Doppler observation associated with magnetic storm. J Atmos Terr Phys 36:2047–2053. https://doi.org/10.1016/0021-9169(74)90192-5

Ichinose T, Ogawa T (1976) Internal gravity waves deduced from the HF Doppler data during the April 19, 1958, solar eclipse. J Geophys Res 81:2401–2404. https://doi.org/10.1029/JA081i013p02401

Ivanov DV, Ivanov VA, Ryabova NV, Elsukov AA, Ryabova MI, Chernov AA (2015) System of frequency providing of HF communication channels based on the new digital sounder on USRP platform. T-Comm 9:86–88

Jacobs JA, Watanabe T (1966) Doppler frequency changes in radio waves propagating through a moving ionosphere. Radio Sci 1(3):257–264. https://doi.org/10.1002/rds196613257

Kato Y, Saito T (1958) Investigation on the magnetic disturbance by the induction magnetograph, Part VII. on the damped type rapid pulsation accompanying ssc. science reports of the Tohoku University Ser 5. Geophysics 9:99–112

Kester W (2005) The data conversion handbook. Newnes, Burlington

Kikuchi T (1986) Evidence of transmission of polar electric fields to the low latitude at times of geomagnetic sudden commencements. J Geophys Res 91:3101–3105. https://doi.org/10.1029/JA091iA03p03101

Kikuchi T, Araki T (1979) Horizontal transmission of the polar electric field to the equator. J Atmos Terr Phys 41:927–936. https://doi.org/10.1016/0021-9169(79)90094-1

Nakata *et al. Earth, Planets and Space*   (2021) 73:209

Page 16 of 16

Kikuchi T, Hashimoto KK (2016) Transmission of the electric fields to the low latitude ionosphere in the magnetosphere-ionosphere current circuit. Geosci Lett 3:1–11. https://doi.org/10.1186/s40562-016-0035-6

Kikuchi T, Ishimine T, Sugiuchi H (1985) Local time distribution of HF Doppler frequency deviations associated with storm sudden commencements. J Geophys Res 90:4389. https://doi.org/10.1029/ja090ia05p04389

Kikuchi T, Lühr H, Kitamura T, Saka O (1996) Direct penetration of the polar electric field to the equator during a DP 2 event as detected by the auroral and equatorial magnetometer chains and the EISCAT radar. J Geophys Res Space Phys 101:17161–17173. https://doi.org/10.1029/96JA01299

Kikuchi T, Hashimoto KK, Tomizawa I, Ebihara Y, Nishimura Y, Araki T, Shinbori A, Veenadhari B, Tanaka T, Nagatsuma T (2016) Response of the incompressible ionosphere to the compression of the magnetosphere during the geomagnetic sudden commencements. J Geophys Res 121:1536–1556. https://doi.org/10.1002/2015ja022166

Kikuchi T, Chum J, Tomizawa I, Hashimoto KK, Hosokawa K, Ebihara Y, Hozumi K, Supnithi P (2021) Penetration of the electric fields of the geomagnetic sudden commencement over the globe as observed with the HF Doppler sounders and magnetometers. Earth Planets Space 73:10. https://doi.org/10.1186/s40623-020-01350-8

Laštovička J, Chum J (2017) A review of results of the international ionospheric Doppler sounder network. Adv Space Res 60:1629–1643. https://doi.org/10.1016/j.asr.2017.01.032

Liu JY, Chen CH, Sun YY, Chen CH, Tsai HF, Yen HY, Chum J, Lastovicka J, Yang QS, Chen WS, Wen S (2016) The vertical propagation of disturbances triggered by seismic waves of the 11 March 2011 M 9.0 Tohoku earthquake over Taiwan. Geophys Res Lett 43:1759–1765. https://doi.org/10.1002/2015gl067487

Motoba T, Kikuchi T, Shibata TF (2004) HF Doppler oscillations in the low-latitude ionosphere coherent with equatorial long-period geomagnetic field oscillations. J Geophys Res 109:A06214. https://doi.org/10.1029/2004JA010442

Nakata H, Takaboshi K, Takano T, Tomizawa I (2021) Vertical propagation of coseismic ionospheric disturbances associated with the foreshock of the Tohoku Earthquake observed using HF Doppler sounding. J Geophys Res. https://doi.org/10.1029/2020JA028600

Nishitani N, Ruohoniemi JM, Lester M, Baker JBH, Koustov AV, Shepherd SG, Chisham G, Hori T, Thomas EG, Makarevich RA, Marchaudon A, Ponomarenko P, Wild JA, Milan SE, Bristow WA, Devlin J, Miller E, Greenwald RA, Ogawa T, Kikuchi T (2019) Review of the accomplishments of midlatitude Super Dual Auroral Radar Network (SuperDARN) HF radars. Prog Earth Planet Sci 6:27. https://doi.org/10.1186/s40645-019-0270-5

Occhipinti G, Dorey P, Farges T, Lognonné P (2010) Nostradamus: the radar that wanted to be a seismometer. Geophys Res Lett 37:L18104. https://doi.org/10.1029/2010gl044009

Ogawa T (1958) Frequency variations in short-wave propagation. Proc IRE 46:1934–1939. https://doi.org/10.1109/JRPROC.1958.286813

Okuzawa T, Shibata T, Yasui H (1983) On the ionospheric effect of near-source earthquakes around the islands of japan detected by the hf-doppler technique. J Geomagn Geoelectr 35:391–397. https://doi.org/10.5636/jgg.35.391

Okuzawa T, Shibata T, Ichinose T, Takagi K, Nagasawa C, Nagano I, Mambo M, Tsutsui M, Ogawa T (1986) Short-period disturbances in the ionosphere observed at the time of typhoons in september 1982 by a network of HF doppler receivers. J Geomagn Geoelectr 38:239–266. https://doi.org/10.5636/jgg.38.239

Otsuka Y, Onoma F, Shiokawa K, Ogawa T, Yamamoto M, Fukao S (2007) Simultaneous observations of nighttime medium-scale traveling ionospheric disturbances and *E* region field-aligned irregularities at midlatitude. J Geophys Res 112:A06317. https://doi.org/10.1029/2005JA011548

Reddy CA, Ravindran S, Viswanathan KS, Murthy BVK, Rao DRK, Araki T (1994) Observations of Pc5 micropulsation-related electric field oscillations in the equatorial ionosphere. Ann Geophysicae 12:565–573. https://doi.org/10.1007/s00585-994-0565-7,1994

Reinisch BW, Galkin IA, Khmyrov GM, Kozlov AV, Bibl K, Lisysyan IA, Cheney GP, Huang X, Kitrosser DF, Paznukhov VV, Luo Y, Jones W, Stelmash S, Hamel R, Grochmal J (2009) New Digisonde for research and monitoring applications. Radio Sci. https://doi.org/10.1029/2008rs004115

Reinisch B, Galkin I, Belehaki A, Paznukhov V, Huang X, Altadill D, Buresova D, Mielich J, Verhulst T, Stankov S, Blanch E, Kouba D, Hamel R, Kozlov A, Tsagouri I, Mouzakis A, Messerotti M, Parkinson M, Ishii M (2018) Pilot ionosonde network for identification of traveling ionospheric disturbances. Radio Sci 53:365–378. https://doi.org/10.1002/2017RS006263

Sastri JH, Ramesh KB, Rao DRK, Rao JVSV (1993) Oscillations in F-region Doppler velocity in the dip equatorial region associated with ULF geomagnetic pulsations. J Atmos Terr Phys 55:1271–1280. https://doi.org/10.1016/0021-9169(93)90051-Y

Sastri JH, Luhr H, Tachihara H (2000) Letter to the editor: electric field fluctuations (25–35 min) in the midnight dip equatorial ionosphere. Ann Geophys 18:252–256. https://doi.org/10.1007/s00585-000-0252-2

Shibata T (1986) Two classes of medium-scale traveling ionospheric disturbances observed by an HF Doppler array. J Geomagn Geoelectr 38:779–796. https://doi.org/10.5636/jgg.38.779

Shibata T, Okuzawa T (1983) Horizontal velocity dispersion of medium-scale travelling ionospheric disturbances in the F-region. J Atmos Terr Phys 45:149–159. https://doi.org/10.1016/S0021-9169(83)80019-1

Simi KG, Susanth SG, Sumod SG (2020) On the vector plasma drift measurements over Equatorial Ionosphere using HF Doppler radar–a brief review. Indian J Sci Technol 13:3642–3651. https://doi.org/10.17485/IJST/v13i35.1084

Skolnik MI (1990) Radar handbook. McGraw-Hill, New York

Tomizawa I, Shibata T, Okuzawa T, Arisawa T, Seo Y, Adachi N (2003) Development of HF transmission system specialized for ionospheric disturbance observation. Bull Univ Electro-Commun 16:83–93

Tsutsui M, Ogawa T, Kamide Y, Kroehl HW, Hausman BA (1988) A method of estimating horizontal vectors of ionospheric electric field deduced from HF Doppler data. Radio Sci 23:119–128. https://doi.org/10.1029/RS023i002p00119

Yokoyama T, Hysell DL, Otsuka Y, Yamamoto M (2009) Three-dimensional simulation of the coupled Perkins and E_s-layer instabilities in the nighttime midlatitude ionosphere. J Geophys Res 114:A03308. https://doi.org/10.1029/2008JA013789

Publisher's Note